PCCP

PAPER

Cite this: *Phys. Chem. Chem. Phys.*, 2019, **21**, 12530

Molecular mechanisms of pore formation and membrane disruption by the antimicrobial lantibiotic peptide Mutacin 1140†

Rudramani Pokhrel, [a] Nisha Bhattarai, [a] Prabin Baral, [a] Bernard S. Gerstman, [ab] Jae H. Park, [c] Martin Handfield [c] and Prem P. Chapagain *[ab]

The emergence of antibiotic-resistance is a major concern to global human health and identification of novel antibiotics is critical to mitigate the threat. Mutacin 1140 (MU1140) is a promising antimicrobial lanthipeptide and is effective against Gram-positive bacteria. Like nisin, MU1140 targets and sequesters lipid II and interferes with its function, which results in the inhibition of bacterial cell wall synthesis, and leads to bacteria cell lysis. MU1140 contains a structurally similar thioether cage for binding the lipid II pyrophosphate as for nisin. In addition to lipid II binding, nisin is known to form membrane pores. Membrane pore formation and membrane disruption is a common mode of action for many antimicrobial peptides, including gallidermin, a lantibiotic peptide with similar structural features as MU1140. However, whether and how MU1140 and its variants can form permeable membrane pores remains to be demonstrated. In this work, we explored the potential mechanisms of membrane pore formation by performing molecular simulations of the MU1140–lipid II complex in the bacterial membrane. Our results suggest that MU1140–lipid II complexes are able to form water permeating membrane pores. We find that a single chain of MU1140 complexed with lipid II in the transmembrane region can permeate water molecules across the membrane *via* a single-file water transport mechanism. The ordering of the water molecules in the single-file chain region as well as the diffusion behavior is similar to those observed in other biological water channels. Multiple complexes of MU1140–lipid II in the membrane showed enhanced permeability for the water molecules, as well as a noticeable membrane distortion and lipid relocation, suggesting that a higher concentration of MU1140 assembly in the membrane can cause significant disruption of the bacterial membrane. These investigations provide an atomistic level insight into a novel mode of action for MU1140 that can be exploited to develop optimized peptide variants with improved antimicrobial properties.

Received 20th March 2019,
Accepted 20th May 2019

DOI: 10.1039/c9cp01558b

rsc.li/pccp

I. Introduction

The emergence of antibiotic-resistant variants of pathogenic bacteria has posed a major threat to human health.[1] Discovery of novel antibiotics, especially those with novel mechanisms of action, is critical to mitigate the threat of antibiotic-resistance.[2] Antibiotics containing lanthionine, referred to as lantibiotics,[3] constitute a promising class of drugs to battle the threat of antibiotic resistance. These cationic antimicrobial peptides are effective against Gram-positive bacteria which have negatively charged membrane surfaces.[4,5] Most of the current antimicrobial peptides target bacterial cell membrane. The amphipathic nature of many antimicrobial peptides allows them to interact with both the hydrophobic tail as well as hydrophilic phospholipid groups.[6] Some antimicrobial peptides such as mutacin and nisin target lipid II which is essential for bacterial cell wall synthesis.[5,7,8] Lipid II transports peptidoglycan subunits from the cytoplasm to the outside of the bacterium to form the peptidoglycan matrix which is the main component of the cell wall.[9] Thus, these antimicrobial peptides interfere with the function of lipid II and inhibit the cell wall synthesis, ultimately leading to bacteria stasis or lysis.

Lipid II has two binding moieties for antimicrobial peptides. One is the peptide moiety that is the target for current clinical drugs, including vancomycin, and the other moiety is the pyrophosphate group targeted by several lantibiotics.[10] Resistant strains

[a] *Department of Physics, Florida International University, Miami, FL 33199, USA. E-mail: chapagap@fiu.edu*
[b] *Biomolecular Sciences Institute, Florida International University, Miami, FL 33199, USA*
[c] *Oragenics Inc, Alachua, FL, USA*

† Electronic supplementary information (ESI) available. See DOI: 10.1039/c9cp01558b

of bacteria have been able to change peptide composition in a way that impedes the binding ability of antibiotics that target the peptide moiety but without affecting the cell wall synthesis. For example, lipid II mutations in the peptide moiety rendered vancomycin ineffective by destabilizing the vancomycin–lipid II complex.[11,12] Interestingly, the composition of the pyrophosphate moiety has remained unaltered through evolution, even in the presence of a significant selective pressure resulting from the widespread use of antibiotics. Therefore, it is worthwhile to focus on the development of novel antibiotics that target the phosphate moiety of lipid II. This emphasizes the importance of research on lantibiotics to develop the next generation antibiotics to tackle antibiotic-resistant pathogens.

The most extensively studied lantibiotic compound is nisin. It is proposed that the antimicrobial activities of nisin are attributed to two modes of action: (1) vancomycin-like blockage of the peptidoglycan synthesis by binding to and abduction of lipid II and (2) membrane pore formation.[8,13–15] For nisin, the first mechanism has been well established, while the second mechanism has attracted interest in the field. Very recently, an NMR study conclusively showed that compared to the solution state, the nisin–lipid II complex is drastically different in the pharmacologically relevant membrane environment where nisin forms a pore complex with lipid II in membranes.[16,17] Although nisin has been an effective antimicrobial peptide and used as a food preservative for decades, its degradability and toxicity, along with other immunogenicity and pharmacokinetic issues have limited its use as an antibiotic drug.[18] Therefore, alternate and optimized lantibiotics that are more suitable for clinical use are highly sought after. One such compound that has emerged as a promising lantibiotic is Mutacin 1140 (MU1140). Mutacin 1140 is naturally produced by the Gram-positive bacterium *Streptococcus mutans*[19] and possesses low levels of toxicity, good pharmacokinetics, and a high level of stability.[20,21]

Recently, at least 17 variants of MU1140 were identified with equal or superior *in vitro* susceptibility profiles against the Gram-positive pathogen *C. difficile* in animal model, compared to vancomycin.[20,22,23] The stability and efficacy of MU1140 can be enhanced by the replacement of amino acids of its chain.[20,24] Similar to nisin, MU1140 is believed to traffic lipid II, thereby interfering with bacterial cell wall synthesis.[5,25] Mutacin-1140 contains a structurally similar thioether A/B rings as in nisin that provide the binding cage for the pyrophosphate of lipid II and therefore also binds with lipid II. It is shown that nisin complexed with lipid II can form membrane pores.[16,17] Similarly, gallidermin, a lantibiotic that is structurally similar to, and the same length as MU1140 (22 amino acids long), has been shown to form functional membrane pores that depolarize DOPC/DPoPC membranes, likely by allowing sodium and/or potassium to diffuse through the membrane.[26] Its ability to form pores correlates with the membrane thickness and composition; *i.e.* the less thick the membrane is, the more likely it is to result in pore formation.[26] In addition to these, pore formation is a common mode of action for most antimicrobial peptides.[27] However, early work on MU1140 suggested that it may not form functional membrane pores because of its size.[19,25] Therefore, whether and how MU1140 and its variants could form the permeable membrane pores remains to be determined. In this work, we explored the potential mechanism of membrane pore formation by performing molecular dynamics (MD) simulations of the MU1140–lipid II complex in the bacterial membrane. Despite significant structural/sequence differences between the nisin and MU1140 C-terminal tails, our results show that MU1140–lipid II complexes are able to form functional, water permeating membrane pores. These investigations, for the first time, provide an atomistic level insight into a novel mode of action for MU1140 that can be exploited to develop optimized peptide variants with improved antimicrobial properties and therapeutic profile.

II. Methods

1. Molecular model of Mutacin 1140–lipid II complex

The NMR structure of the nisin–lipid II complex (PDB ID 1wco) was used as a template to model the MU1140–lipid II complex (Fig. 1), preserving the structure of the pyrophosphate binding cage and the lantibiotic–lipid II interactions. With the target being the pyrophosphate moiety, a dipeptide (Ala, Glu) was

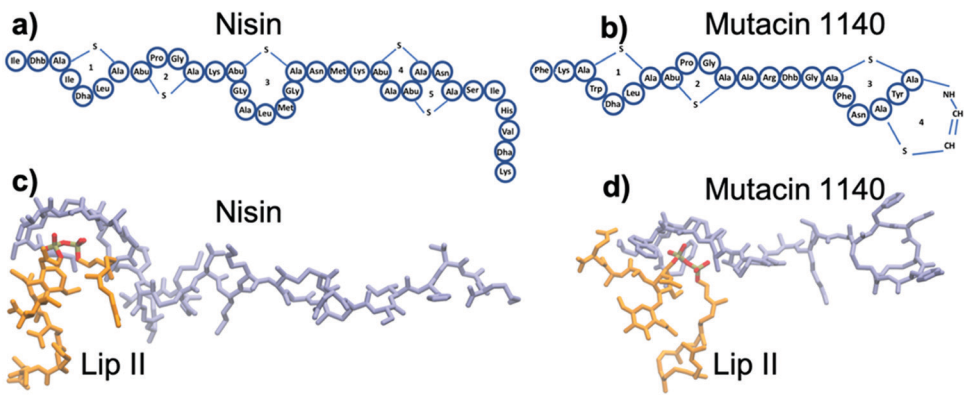

Fig. 1 Schematic representation of amino acid sequences of (a) nisin and (b) MU1140 chains. The NMR structure of (c) the nisin–lipid II complex[8] and (d) the modeled structure of the MU1140–lipid II complex. The lantibiotic chains are shown in blue and lipid-II in orange. The phosphate and oxygen atoms in the pyrophosphate moiety are highlighted in gray and red respectively.

used for the peptide moiety and a longer bactoprenol tail was used that provided a stable anchorage during membrane-lipid II simulation.

2. Molecular dynamics simulations

We used two different types of membrane systems: (1) a highly mobile membrane-mimetic (HMMM) model[28] for investigating membrane insertion and (2) an all-atom membrane with full-length lipids for investigating the membrane pore mechanics. The membrane system was generated using the CHARMM-GUI membrane builder web server.[29] The lipid bilayer contained POPE and POPG lipids in the ratio of 1 : 3 to represent the membrane of Gram-positive bacteria.[30] For the HMMM model membrane system, the MU1140–lipid II complex was placed in the membrane in such a way that MU1140 lies horizontally at the outer surface of the lipid bilayer and lipid II orients perpendicularly (*i.e.* parallel to other lipids) in the lipid bilayer. For the membrane system with full-length lipids, MU1140 is placed in the transmembrane region, parallel to lipid II. The HMMM membrane system was run for 1.3 μs, whereas the full-length lipid membrane system was run for 0.5 μs. For the membrane with full-length lipids, we set up three different membrane pore systems containing one, two, and four units of the MU1140–lipid II complex respectively. Each of these complexes were run for 500 ns of MD simulations. In addition, simulations of each of these three complexes were repeated and run again for 500 ns each. The simulations performed for various systems are summarized in Table S1 (ESI†).

The force field parameters for the dehydrated amino acids Dha, Dhb, and Abu were taken from previous work on nisin by Turpin *et al.*[31] The CHARMM36m[32] force field was used for all MD simulations using NAMD 2.12[33] with a time step of 2 fs. The minimization and equilibration dynamics of the membrane system were performed in accordance with the 6-step protocol. Periodic boundary conditions were employed in all simulations. The long-range electrostatic interactions were treated using the particle mesh Ewald (PME) method. To constrain the covalent bonds involving hydrogen atoms, the SHAKE algorithm was used. A Nose–Hoover Langevin-piston method was used with a piston period of 50 fs and a decay of 25 fs to control the pressure. All simulations were run at 300 K temperature with Langevin temperature coupling and a friction coefficient of 1 ps^{-1}. For calculations of hydrogen bonds, the cut-off distance and cut-off angle were 3.5 Å and 30° respectively. The visualization tool VMD[34] was used to visualize the trajectories and render the pictures.

III. Results

1. Structural comparison of MU1140 and nisin

As with other lantibiotics chains, MU1140 contains unsaturated amino acid residues dehydroalanine (Dha), dehydrobutyrine (Dhb), aminobutyric acid (Abu), and a C-terminal aminovinyl-D-cysteine (AviCys). It contains thioether rings connecting two amino acids by a sulfur bridge, with Ala-S-Ala as the lanthionine derivative (Lan) and Abu-S-Ala as the 3-methyl-lanthionine (MeLan) derivative. Conserved disulfide-bonds are found in a wide range of amphiphilic antimicrobial peptides and viroporins, and are important for membrane insertion and their pore-forming.[35–37] In Fig. 1, we compare the sequence and structure of the nisin and MU1140 chains. Compared to the 34-residue nisin, MU1140 is shorter, with only 21 amino acids. Nisin contains five thioether rings, whereas MU1140 contains three thioether rings and a forth ring formed by heteroatoms at the C-terminal tail (Fig. 1a and b).

Nisin has three Lys residues giving a net 3+ charge (excluding the N-terminus group). In contrast, MU1140 contains a net 2+ charge due to two basic amino acids Lys and Arg. The anionic pyrophosphate moiety of lipid II with a net 2− charge provides the binding target for the cationic MU1140. The hydrophilic head group of lipid II consists of two sugar linked rings *N*-acetyl-glucosamine (GlcNAc), *N*-acetylmuramic acid (MurNAc), and pentapeptides connected to MurNAc.[5,9,10] The hydrophobic tail, bactoprenol is linked to MurNac *via* a pyrophosphate moiety. The lipid II binding thioether rings in nisin and MU1140 (positions 3–11) are nearly identical, with only one amino acid difference (Ile *vs.* Trp in position 4). Therefore, we used the structure of the nisin–lipid II complex (PDB ID 1wco) as a template for modeling the MU1140–lipid II complex, preserving the structure of the pyrophosphate binding cage and the lantibiotic–lipid II interactions. The NMR structure of the nisin–lipid II[8] complex I is shown in Fig. 1c and our model for the MU1140–lipid II complex (energy minimized and equilibrated structure) is shown in Fig. 1d.

2. MU1140 interactions with the membrane surface and lipid II

To investigate the interactions of MU1140 chain with the membrane surface when it is bound with lipid II in the membrane, we placed the MU1140–lipid II complex in the membrane in such a way that the MU1140 chain lies horizontally on the outer surface of the lipid bilayer, and the lipid II is inserted into the membrane, aligned parallel with other lipids in the lipid bilayer (Fig. 2a). The MU1140-membrane surface interactions are relevant not only for its lipid II trafficking mechanism but also for the initial phase of the peptide insertion into the membrane. We performed a 500 ns simulation of the complex in the bacterial membrane composed of POPE and POPG in the ratio of 1 : 3.

We observed that the MU1140–lipid II complex remained intact throughout the simulation, with strong interactions between MU1140 and the pyrophosphate moiety of lipid II. At the end of the 500 ns simulation, residues in the third thioether ring as well as the C-terminal segment show partial insertion into the membrane bilayer (Fig. 2a). In Fig. 2b, we plot the percentage of time during the MD simulation that major amino acids in MU1140 form hydrogen bonds with the membrane as well as with lipid II (inset).

The MU1140 cationic side chain of Lys2 makes the major salt-bridge interaction and the backbone NH groups of Phe1 and Lys2 provide strong hydrogen bonding with the pyrophosphate group in lipid II (Fig. 2b, right). As displayed in Fig. 2c, MU1140 makes approximately three salt-bridge or hydrogen bonds interactions with lipid II throughout the simulation.

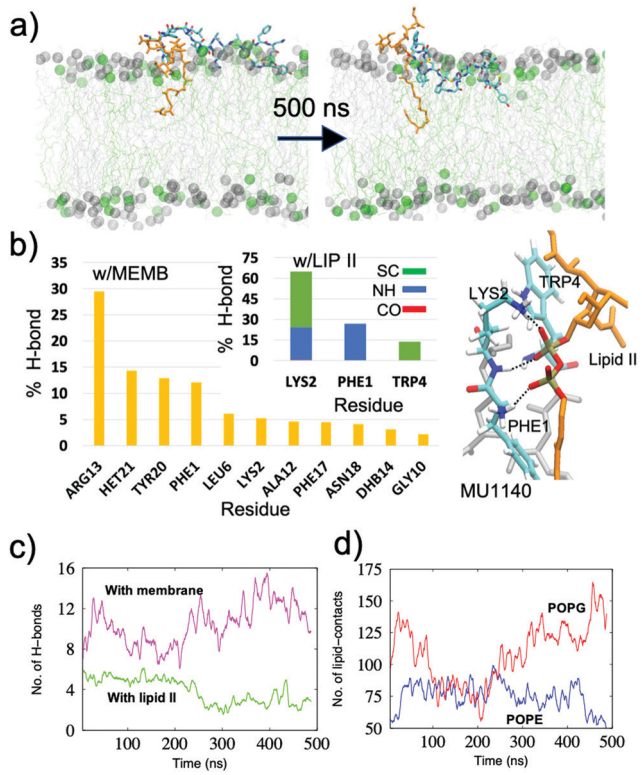

Fig. 2 (a) MU1140–lipid II complex in the membrane at 0 ns and 500 ns. MU1140 is colored in by atom names, lipid II in orange, POPE in green, and POPG in gray. The phosphorous atoms in the lipid headgroups are shown as spheres. (b) Percentage hydrogen bonds between MU1140 and membrane as well as between MU1140 and lipid II (inset). The % H-bond between MU1140 and lipid II are colored as, green: sidechain (SC), blue: backbone NH group, and red: backbone CO group. Important MU1140 residues participating in hydrogen bonding with lipid II are highlighted (right). (c) Number of hydrogen bonds of MU1140 with lipid II as well as with other lipids in the membrane as a function of time. (d) Number of lipid contacts with MU1140 as a function of time.

In addition, the bar graph for the MU1140-membrane hydrogen bond in Fig. 2b shows that MU1140 is able to strongly interact with the bacterial membrane surface through significant hydrogen bonding. The major MU1140-membrane hydrogen bond contribution comes from the MU1140 Arg13, followed by the hetero-group (AviCys) at the C-terminal tail and the backbone interactions of Tyr20. Overall, MU1140 makes about 12 hydrogen bonds on average with the membrane, as shown in Fig. 2c. In Fig. 2d, we plotted the number of MU1140 contacts with lipid II within 3.5 Å. MU1140 has a nearly constant number of interactions with POPE throughout the simulation, whereas interactions with POPG shows a slight increase after 200 ns.

As a control, we performed a separate simulation for the MU1140 chain on the membrane surface while it is not complexed with lipid II. As shown in Fig. S1 (ESI†), the MU1140 chain interacts with the membrane surface but the partial insertion of the hydrophobic groups is not as pronounced as in MU1140 complexed with lipid II (Fig. 2a). This suggests that the lipid II interactions in the pyrophosphate moiety allows the MU1140 chain to stabilize on the membrane surface and facilitate membrane insertion.

3. Membrane insertion of MU1140

A net cationic charge and a high fraction of the hydrophobic residues are two common features of antimicrobial peptides (AMPs)[38] and the hydrophobicity can allow the peptide chain to insert into the membrane. MU1140's close analogs, nisin and gallidermin are both shown to form membrane pores.[16,17,26] Based on the similarities of lipid II binding and the peptide composition with respect to nisin, epidermin, and gallidermin, we conjectured that MU1140 can also form functional membrane pores. The observation of peptide insertion in an all-atom computational model is difficult due to temporal limitations of unbiased MD simulations. A 500 ns of detailed all-atom simulation with full-length lipids allowed only a partial insertion of MU1140. To facilitate the membrane insertion in reasonable computational timescales, we used a highly mobile membrane-mimetic (HMMM) model.[28] The HMMM membrane model uses lipids with shortened tails, floating on a layer of 1,1-dichloroethane (DCLE) representing the hydrophobic inner core of the lipid bilayer. The fluidity of the system allows significantly enhanced lipid diffusion that can provide unbiased lipid-binding of the protein well under a microsecond. With the MU1140 chain aligned along the membrane surface (Fig. 3a) and the lipid II aligned parallel to the lipids, we performed a production run for 1.3 μs. Fig. 3a shows the configuration of the complex in the beginning of the simulation (left panel) and after 1 μs of simulation (right panel). Fig. 2b shows the vertical distance (*z*-axis) between Tyr20 and the center-of-mass of the lipid bilayer (representing the lipid bilayer's mid-point). After about 800 ns, the MU1140 chain begins to insert into the membrane and by around

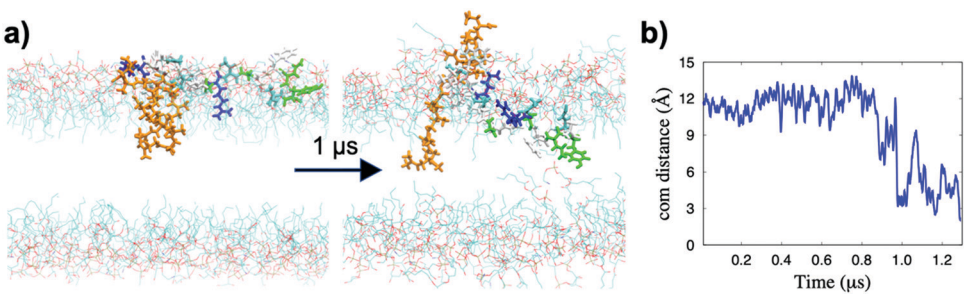

Fig. 3 (a) Insertion of MU1140 into the HMMM membrane. For clarity, DCLE molecules in the transmembrane region are not shown. (b) Distance between the Tyr20 of MU1140 and the center-of-mass (com) of the lipid bilayer (membrane mid-point).

1 μs, most of the chain that is not interacting with the lipid II pyrophosphate cage is in the transmembrane region, as can be seen in Fig. 3a (right) and the decreasing distance from the lipid bilayer's mid-point in Fig. 3b. These results show that the MU1140 chain prefers the hydrophobic transmembrane region compared to the outer surface of the membrane.

4. Membrane pore formation and water permeation by MU1140

After confirming that the hydrophobic transmembrane region is a favorable environment for the MU1140 chain, we investigated its pore forming ability. While insertion is greatly facilitated by the HMMM membrane, the inserted MU1140 chain is indifferent towards aligning in any specific orientation because of the fluidity of the transmembrane DCLE that does not restrict the peptide chain to a vertical orientation as the full-length lipids would. Therefore, investigation of the pore formation requires a bilayer with full-length lipids. One way to set this up is to wait for a random even that vertically orients the MU1140 chain in the HMMM membrane and then add the lipid tails. To expedite this process, we set-up a MU1140–lipid II complex in a conventional lipid bilayer with full-length lipids but with the MU1140 already inserted and aligned vertically in the transmembrane region. We note that use of enhanced sampling methods such as accelerated molecular dynamics may allow investigations of membrane insertion without having to reset the system.

Fig. 4a shows the initial configuration of the MU1140–lipid II complex in the bacterial membrane composed of POPE and POPG in the 1 : 3 ratio. We performed a 500 ns simulation for the system and observed a significant water permeation even with a single complex of MU1140 and lipid II. Fig. 4b shows a representative frame at the end of the 500 ns simulation which shows water molecules along the MU1140 chain in the transmembrane region.

Before the simulation began, only the N-terminal part of the peptide is exposed to water on the outside of the bacterial membrane and the C-terminal is buried in the transmembrane region as shown in Fig. 4. Within a 100 ns, the lower end of MU1140 inside the membrane is in contact with water molecules below the membrane (intracellular space). Despite having a significantly shorter chain compared to nisin, MU1140 is able to span the transmembrane region and create a channel for water permeation. As with gallidermin that also harbors a shorter chain, the water permeation and pore formation by MU1140 likely correlates with the membrane thickness.[26] The bactoprenol tail of lipid II has no particular preference in its orientation and is quite flexible in the transmembrane region. Although lipid II interactions may facilitate membrane insertion of MU1140, simulations of MU1140 chain (not complexed with lipid II) in the transmembrane region showed similar water permeation behavior (Fig. S2, ESI†).

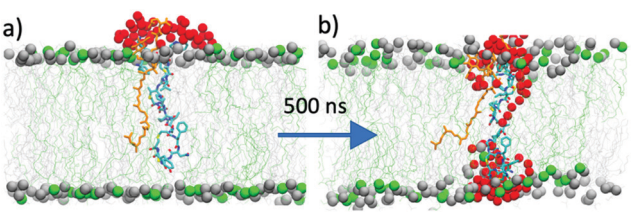

Fig. 4 MU1140–lipid II complex in a bacterial membrane: (a) initial configuration of the complex and (b) a configuration at the end of 500 ns simulation. The phosphorus atoms of POPE are highlighted as green spheres and that of POPG as gray sphere. The water molecules within 4 Å of the peptide are highlighted as red spheres.

5. Single-file water permeation

To explore the mechanism of water permeation, we examined the residues and the groups involved in interactions with water. We created a list of all water molecules that come within 3.5 Å of peptide residues and calculated the number of hydrogen bonds between the peptide and water. Fig. 5 displays a snapshot of a typical frame that shows a single-file water permeation between the outer and inner layers of the membrane. Movie S1 (ESI†) shows how water molecules permeate across the bilayer *via* hydrogen bonding with MU1140 residues. Single-filed hydrogen bonded chains of water are often observed in nanoscale confinements such as in carbon nanotubes and protein channels (*e.g.*, the aquaporin gramicidin)[39,40] and are of great interest because of their unusual properties. As shown in Fig. 5, water molecules in the single-file chain region are considerably ordered, similar to the behavior observed in other biological water channels such as gramicidin A.[41,42] The importance of the single-file water is underscored by its role in transporting ions. In gramicidin A, the ability of single-file water to stabilize K^+ ions and transport it through the channel is due to the solvation of the ion by two single file chains on either side.[43,44] Unlike fully non-polar carbon nanotubes, biological water pores are lined with backbone carbonyl and amide groups that can form hydrogen bonds with water molecules. As here, water molecules in the single-file region predominantly hydrogen-bond with carbonyl groups of MU1140 residues. With larger

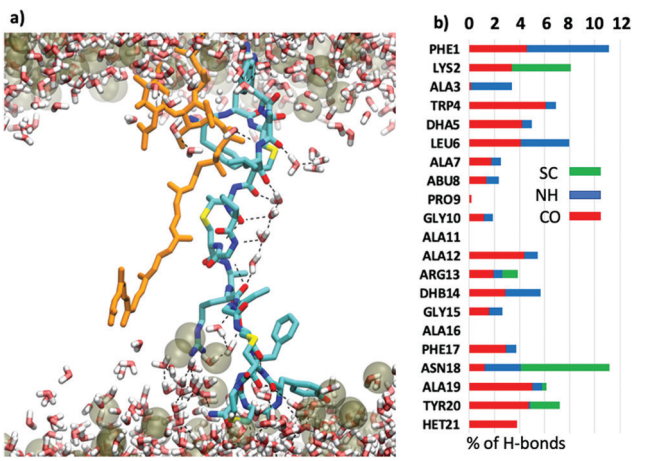

Fig. 5 (a) A representative snapshot of the water permeation along the MU1140 chain (cyan) in the transmembrane region. Lipid II is shown in orange. (b) Percentage of hydrogen-bonding between MU1140 residues and water molecules, showing MU1140 hydrogen bonds with backbone CO (red), backbone NH (blue), and sidechain (SC) (green). Only the phosphate atoms of the lipids are displayed for clarity.

assembly of MU1140–lipid II complexes, transport of cations may be possible because the polar lining by the backbone carbonyl groups in MU1140 may form hydrogen bonding with monovalent cations and facilitate ion transport as shown for epidermin and gramicidin.[45]

The MU1140 structure inside the membrane shows a concaving at and below the second thioether ring and this allows a proper orientation of CO and NH groups of MU1140 residues so that the water molecules can line along the chain (Fig. 5a). We calculated the % hydrogen bond between MU1140 groups and water molecules and plotted the results in Fig. 5b. Three residues Pro9, Ala11, and Ala16 are oriented away and make almost no contacts with water. Since Phe1 and Asn18 are close to the bulk water, they are found to form the most hydrogen bonds with water. While only the backbone groups of Phe1 are involved in hydrogen bonding, Asn18 sidechain makes significant hydrogen bonding with water. It is found that substitution of Phe1 with other resides does not negatively impact MU1140 activity[46,47] possibly because backbone hydrogen bonding is unaffected. Based on the hydrogen bonding pattern, three different transmembrane regions can be observed along the chain: (1) residues 1–5, (2) residues 6–13, and (3) residues 14–18. Along the sequence Leu6 to Arg13, considerably ordered single-file water is observed. The MU1140 hydrogen-bonding with the single-file water is found to be with Leu6 (CO), Ala7 (CO), Abu8 (CO), Gly10 (NH), and Arg13 (CO). Due to irregular ordering of backbone carbonyl and amide groups, water passage below Ala12/Arg13 to the bulk occurs in a less ordered fashion and can involve a sequence of as many as four water molecules hydrogen bonded between Ala12 and Phe17. Due to the proximity to the bulk water, the Phe1 to Dhb5 as well as Asn18 to HET21 have the water that is less ordered.

Significant water ordering and hydrogen bonding around the mid-region of the lipid bilayer causes a longer residence times for the water molecules, with major bottlenecks for the ion passage at Leu6 and Arg13. In Fig. 6, we plotted the trajectory for a few representative water molecules that successfully permeated along the z-axis across the lipid bilayer. Water transport is observed in both directions. The concavity of the MU1140 in the mid-region allows relatively more extensive hydrogen bonding for the water molecules. We also plotted the histogram from all the successful trajectories (right panel), which shows a significantly populated mid-region (left panel). This is consistent with the observations in other biological systems which show markedly reduced diffusion of water with the increase in hydrogen bonds with the pore-lining residues.[47] When the single-file water molecules hydrogen bonds with the pore-lining residues, water movement is limited due to the time it takes to not only break the hydrogen bonds but also to reorient and form new hydrogen bonds while moving through the channel. In fact, Horner *et al.*[47] found that the flow of single-file water depends more on the number of hydrogen bonds with pore-lining residues than the channel geometry. In contrast, the hydrophobic walls of carbon nanotubes can allow unrestricted water flow.[39,40] In addition to the role of polar groups lining the pore wall, water permeation across the membrane is also limited by the dehydration penalty at the pore entrance. The fairly low population of water at the two extremes (*i.e.* $|z| > 15$ Å in Fig. 6) is likely due to this penalty. The two least populated regions (before Leu6 and after Arg13) represent the transition states for the water passage.

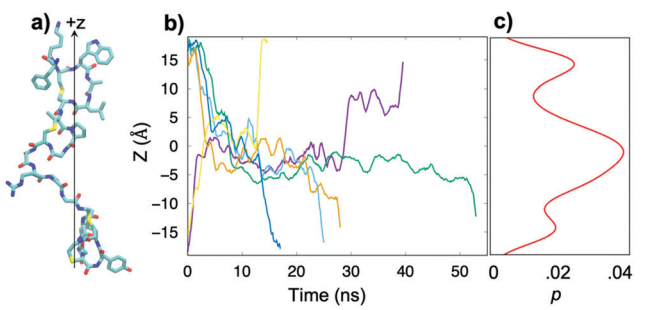

Fig. 6 (a) MU1140 orientation in the lipid bilayer along z-axis (b) representative trajectories of successful water permeation across the membrane. (c) A histogram of the number of water molecules along z-axis is shown on the side.

From the successful water permeation trajectories, we extracted the first passage times for the water molecules to fully traverse the lipid bilayer. The mean first passage time (MFPT) for the water molecule was found to be $\sim$23 ns, giving a diffusion constant of $D \approx 0.03$ nm^2 ns^{-1} (*i.e.* 3×10^{-7} cm^2 s^{-1}) which is two orders of magnitude slower than the water diffusion in nonpolar carbon nanotubes with $D \approx 3 \times 10^{-5}$ cm^2 s^{-1}.[40,48] Here, the diffusion constant was calculated[48] using $D = L^2/12t$, where $L = 2.8$ nm is the channel length and $\langle t \rangle = 23$ ns is the first passage time. The diffusion constant is similar to the values determined for other biological single file water channels such as aquaporin-1 ($D \approx 4 \times 10^{-7}$ cm^2 s^{-1}),[47] and gramicidin ($D \approx 3 \times 10^{-7}$ cm^2 s^{-1}).[49]

6. Water permeation in multimeric assembly of MU1140–lipid II complexes

In many membrane binding and pore-forming amphipathic peptides, pore formation occurs only if the peptide concentration exceeds certain threshold values.[50] In a physiological environment, multiple MU1140 and lipid II molecules are likely to assemble in the membrane. While nisin has 1 : 1 binding stoichiometry in solution,[51] it is suggested to form membrane pores with a 2 : 1 ratio of nisin–lipid II assembly.[13] However, there is no information available about MU1140–lipid II assembly. To investigate the multimeric assembly of MU1140–lipid II and the behavior of water permeation, we set up additional systems with two and four MU1140–lipid II complexes in the bacterial membrane. Both systems were run for 500 ns each. For each set up, MU1140–lipid II complexes were placed in the membrane with lipid II chains facing away from each other and MU1140 facing towards each other (Fig. 7). We observed that the MU1140 chains drifted towards each other and water molecules permeated across the lipid bilayer. Movie S2 (ESI†) shows this process for the four-chain system. In Fig. 7, we highlighted (with red spheres) the water molecules within 3.5 Å of MU1140 residues with red spheres. Before the simulation, only a few water molecules above the upper lipid layer are in the vicinity of MU1140. At the end of the 500 ns simulations, both the two-chain system and the four chains systems show significant water in the transmembrane

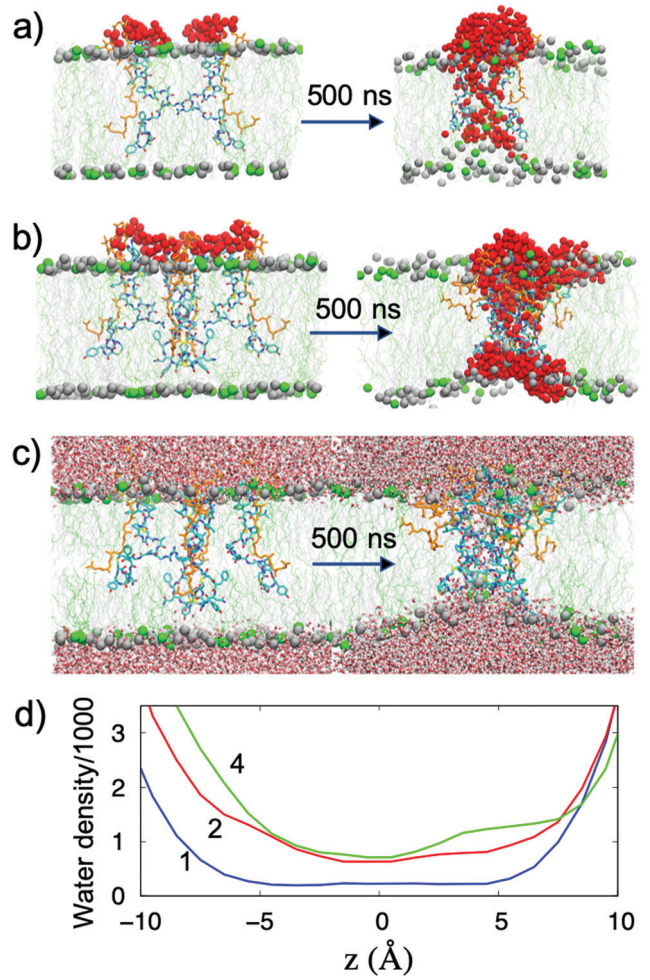

Fig. 7 Assemblies of (a) two and (b) four complexes of MU1140–lipid II in the bacterial membrane at the beginning and end of the 500 ns simulations. MU1140 chains are colored by residue types, lipid II chains are highlighted in yellow, and the water molecules within 3.5 Å of MU1140 are highlighted as red spheres. As in Fig. 4, the phosphorus atoms of POPE are shown as green spheres and POPG phosphorous atoms as gray spheres. (c) Same as (b) but showing the water molecules above and below the lipid layers. The membrane is tapered near the MU1140–lipid II assembly due to the short length of MU1140. (d) Density profile of the water molecules in the transmembrane region of the lipid bilayer for one, two, and four complexes of MU1140–lipid II.

region. Interestingly, the lipid molecules near the MU1140–lipid II complexes were pulled inward. The four MU1140–lipid II complexes show a significant shrinkage or distortion in the membrane thickness (Fig. 7b and c). Due to the short length of MU1140, the membrane is noticeably tapered near the MU1140–lipid II assembly. This is also displayed by the number density of water molecules which shows a narrowing of the density profile with the increase in the number of MU1140 chains (Fig. 7d). Fig. 7d also shows a significantly higher population of water molecules in the transmembrane region for the two and four complexes. An independent, additional set of simulations for one, two, and four complexes yielded quite similar results of water density profile as well hydrogen bonding pattern (Fig. S3, ESI†). Here, the number density of water molecules is calculated using the density profile plugin in VMD[52] and represents the number of atoms of water divided by the total number of atoms in the system projected along the *z*-axis. The displayed number densities are obtained by averaging over the last 300 ns of the MD trajectories. The membrane distortion/tapering and lipid relocation towards the central region of the lipid bilayer due to the MU1140 assembly in the membrane suggests that a higher concentration of the peptide will cause significant disruption of the bacterial membrane, and provides additional support to the model of Matsusaki–Huang which previously proposed a membrane-thinning effect before the actual poration process takes place for amphiphilic peptides.[53]

For both the two and four complexes, significant hydrogen bonding between the water molecules and MU1140 is observed as shown in Fig. 8. For these complexes, we calculated the percentage hydrogen bonding with water per chain and plotted the result as a bar graph in Fig. 8c. Compared to almost non-existent hydrogen bonding with Ala11 and Ala16 with in a single chain of MU1140 in the membrane, both the two and four chain complexes showed markedly higher hydrogen bonding with these residues. Similarly, Arg13 also showed an increased hydrogen bonding in the two and four MU1140–lipid II complexes. Hydrogen bonding with other residues are found to be similar among systems with one, two, and four complexes. Interestingly, the space between the two and four MU1140 chains allows multiple water molecules to traverse the transmembrane region at the same time, and thus breaks the single-file nature of the water permeation that occurs with only one chain (Fig. 5). We calculated the first passage times for successfully traversing the transmembrane region and plotted their distributions. It is interesting to note that the first passage time distribution for one MU1140–lipid II complex has only one well-defined peak with t = 23 ns but

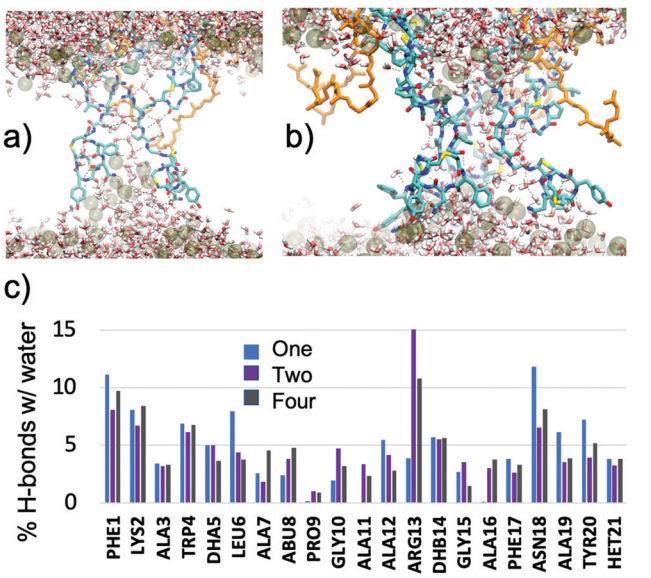

Fig. 8 Representative snapshots of (a) two and (b) four MU1140–lipid II complexes showing water permeation. MU1140 chains are shown in cyan color and lipid II chains are shown in orange. For clarity, only the phosphate atoms of the lipids are displayed. (c) Percentage of hydrogen-bonding per chain for MU1140 and water in the transmembrane region for one, two, and four complexes of MU1140–lipid II.

the distribution for two and four complexes seem to show two different timescales for the water traversing the lipid bilayer: (1) one peak around 22 ns, which is similar to the one chain MU1140 system and likely represents the single-file transportation and (2) the other peak at a much faster timescale ~10 ns, likely from the diffusion in the mid-region.

IV. Conclusions

The ability of MU1140 to bind to the lipid II pyrophosphate moiety and abduct it from the septum of division, therefore obstructing bacterial cell wall synthesis makes it a promising antimicrobial candidate for antibiotic-resistant pathogens. The bacterial-killing mechanisms of certain antimicrobial peptides can be complex and involve more than a single mode of action. For example, it can include interference of the lipid II function and membrane pore formation or membrane disruption. Interestingly, it has been suggested that the lantibiotic spectrum of activity and potency is not necessarily related to the numbers of mechanisms involved. Bonelli *et al.*[53] previously reported that epidermin and gallidermin are 10–20 times more potent against *Lactococcus lactis* than nisin, despite the missing pore formation capacity on that strain. In addition, it was previously shown that [A12L]gallidermin is as active as wild-type gallidermin against *Micrococcus flavus*, despite losing its pore-forming activity.[53] Peptides that have similar moieties and structural features as MU1140, including nisin, epidermin, and gallidermin, have been shown to possess these dual functions in several bacterial strains. However, the molecular mechanisms of how MU1140 and its variants interact with lipid II or form the permeable membrane pores have only been inferred from the structural similarities with nisin and gallidermin. In this work, we explored the interactions of MU1140 with lipid II as well as the mechanism and sequence of membrane pore formation by the MU1140–lipid II complexes in the Gram-positive bacterial membrane using MD simulations. As with nisin, the anionic pyrophosphate moiety of lipid II provides the binding target for the thioether rings in MU1140. The formation of a stable MU1140–lipid II complex highlights the lipid II trafficking mechanism of MU1140 suggested by experimental studies.[8,54,55] Despite structural differences in the C-terminal tail as well as the peptide length between nisin and MU1140, our results show that MU1140–lipid II complexes are able to form functional, water permeating membrane pores. Even a single chain of MU1140 complexed with lipid II is able to permeate water molecules across the membrane *via* a single-file water transport mechanism, which is commonly observed in nanoscale confinement such as carbon nanotubes and protein channels. The ordering of the water molecules in the single-file chain region as well as the diffusion behavior is similar to those observed in other biological water channels such as gramicidin A. Multiple complexes of MU1140–lipid II in the membrane showed enhanced permeability for the water molecules, as well as a noticeable membrane distortion and lipid relocation towards the central region of the lipid bilayer. The results suggest that a higher concentration of MU1140 assembly in the membrane can cause significant disruption of the bacterial membrane. These investigations, for the first time, provide an atomistic level insight into a novel mode of action for MU1140. Further biophysical investigations with different variants of MU1140, lipid compositions, and multimeric assemblies can provide important insights for rational design of optimized peptide variants with improved antimicrobial properties.

Conflicts of interest

JHP and MH had a financial interest in Oragenics as stockholders and employees during the data collection, analysis, and writing of the manuscript.

Acknowledgements

Part of this work was supported by Oragenics Inc.

References

1 A. K. Thabit, J. L. Crandon and D. P. Nicolau, Antimicrobial resistance: impact on clinical and economic outcomes and the need for new antimicrobials, *Expert Opin. Pharmacother.*, 2015, **16**(2), 159–177.
2 S. Sandhaus, P. P. Chapagain and Y. C. Tse-Dinh, Discovery of novel bacterial topoisomerase I inhibitors by use of in silico docking and *in vitro* assays, *Sci. Rep.*, 2018, **8**(1), 1437.
3 J. Z. Acedo, S. Chiorean, J. C. Vederas and M. J. van Belkum, The expanding structural variety among bacteriocins from Gram-positive bacteria, *FEMS Microbiol. Rev.*, 2018, **42**(6), 805–828.
4 B. B. Bonev, W. C. Chan, B. W. Bycroft, G. C. Roberts and A. Watts, Interaction of the lantibiotic nisin with mixed lipid bilayers: a 31P and 2H NMR study, *Biochemistry*, 2000, **39**(37), 11425–11433.
5 H. E. Hasper, N. E. Kramer, J. L. Smith, J. D. Hillman, C. Zachariah, O. P. Kuipers, B. de Kruijff and E. Breukink, An alternative bactericidal mechanism of action for lantibiotic peptides that target lipid II, *Science*, 2006, **313**(5793), 1636–1637.
6 H. Jenssen, P. Hamill and R. E. Hancock, Peptide antimicrobial agents, *Clin. Microbiol. Rev.*, 2006, **19**(3), 491–511.
7 H. Brotz, M. Josten, I. Wiedemann, U. Schneider, F. Gotz, G. Bierbaum and H. G. Sahl, Role of lipid-bound peptidoglycan precursors in the formation of pores by nisin, epidermin and other lantibiotics, *Mol. Microbiol.*, 1998, **30**(2), 317–327.
8 S. T. Hsu, E. Breukink, E. Tischenko, M. A. Lutters, B. de Kruijff, R. Kaptein, A. M. Bonvin and N. A. van Nuland, The nisin–lipid II complex reveals a pyrophosphate cage that provides a blueprint for novel antibiotics, *Nat. Struct. Mol. Biol.*, 2004, **11**(10), 963–967.
9 B. Schwartz, J. A. Markwalder, Y. Wang and I. I. Lipid, Total synthesis of the bacterial cell wall precursor and utilization as a substrate for glycosyltransfer and transpeptidation by penicillin binding protein (PBP) 1b of *Escherichia coli*, *J. Am. Chem. Soc.*, 2001, **123**(47), 11638–11643.

10 D. Munch and H. G. Sahl, Structural variations of the cell wall precursor lipid II in Gram-positive bacteria – Impact on binding and efficacy of antimicrobial peptides, *Biochim. Biophys. Acta*, 2015, **1848**(11 Pt B), 3062–3071.
11 C. T. Walsh, S. L. Fisher, I. S. Park, M. Prahalad and Z. Wu, Bacterial resistance to vancomycin: five genes and one missing hydrogen bond tell the story, *Chem. Biol.*, 1996, **3**(1), 21–28.
12 S. Gardete and A. Tomasz, Mechanisms of vancomycin resistance in Staphylococcus aureus, *J. Clin. Invest.*, 2014, **124**(7), 2836–2840.
13 H. E. Hasper, B. de Kruijff and E. Breukink, Assembly and stability of nisin–lipid II pores, *Biochemistry*, 2004, **43**(36), 11567–11575.
14 I. Wiedemann, E. Breukink, C. van Kraaij, O. P. Kuipers, G. Bierbaum, B. de Kruijff and H. G. Sahl, Specific binding of nisin to the peptidoglycan precursor lipid II combines pore formation and inhibition of cell wall biosynthesis for potent antibiotic activity, *J. Biol. Chem.*, 2001, **276**(3), 1772–1779.
15 I. M. Gut, S. R. Blanke and W. A. van der Donk, Mechanism of inhibition of Bacillus anthracis spore outgrowth by the lantibiotic nisin, *ACS Chem. Biol.*, 2011, **6**(7), 744–752.
16 J. Medeiros-Silva, S. Jekhmane, A. L. Paioni, K. Gawarecka, M. Baldus, E. Swiezewska, E. Breukink and M. Weingarth, High-resolution NMR studies of antibiotics in cellular membranes, *Nat. Commun.*, 2018, **9**(1), 3963.
17 E. Breukink and B. de Kruijff, Lipid II as a target for antibiotics, *Nat. Rev. Drug Discovery*, 2006, **5**(4), 321–332.
18 A. J. van Heel, M. Montalban-Lopez and O. P. Kuipers, Evaluating the feasibility of lantibiotics as an alternative therapy against bacterial infections in humans. Expert Opinion on Drug Metabolism &, *Toxicology*, 2011, **7**(6), 675–680.
19 L. Smith, C. Zachariah, R. Thirumoorthy, J. Rocca, J. Novak, J. D. Hillman and A. S. Edison, Structure and dynamics of the lantibiotic mutacin 1140, *Biochemistry*, 2003, **42**(35), 10372–10384.
20 J. A. Kers, R. E. Sharp, A. W. Defusco, J. H. Park, J. Xu, M. E. Pulse, W. J. Weiss and M. Handfield, Mutacin 1140 Lantibiotic Variants Are Efficacious Against Clostridium difficile Infection, *Front. Microbiol.*, 2018, **9**, 415.
21 O. G. Ghobrial, H. Derendorf and J. D. Hillman, Pharmacodynamic activity of the lantibiotic MU1140, *Int. J. Antimicrob. Agents*, 2009, **33**(1), 70–74.
22 J. A. Kers, A. W. DeFusco, J. H. Park, J. Xu, M. E. Pulse, W. J. Weiss and M. Handfield, OG716: Designing a fit-for-purpose lantibiotic for the treatment of Clostridium difficile infections, *PLoS One*, 2018, **13**(6), e0197467.
23 M. E. Pulse, W. J. Weiss, J. A. Kers, A. W. DeFusco, J. H. Park and M. Handfield, Pharmacological, Toxicological and Dose-Range Assessment of OG716, a Novel Lantibiotic for the Treatment of Clostridium difficile Associated Infection (CDI), *Antimicrob. Agents Chemother.*, 2019, **63**(4), e01904-18.
24 M. Geng and L. Smith, Modifying the Lantibiotic Mutacin 1140 for Increased Yield, Activity, and Stability, *Appl. Environ. Microbiol.*, 2018, **84**, 15.
25 L. Smith, H. Hasper, E. Breukink, J. Novak, J. Cerkasov, J. D. Hillman, S. Wilson-Stanford and R. S. Orugunty, Elucidation of the antimicrobial mechanism of mutacin 1140, *Biochemistry*, 2008, **47**(10), 3308–3314.
26 K. Christ, S. Al-Kaddah, I. Wiedemann, B. Rattay, H. G. Sahl and G. Bendas, Membrane lipids determine the antibiotic activity of the lantibiotic gallidermin, *J. Membr. Biol.*, 2008, **226**(1-3), 9–16.
27 M. Zasloff, Antimicrobial peptides of multicellular organisms, *Nature*, 2002, **415**(6870), 389–395.
28 Y. Qi, X. Cheng, J. Lee, J. V. Vermaas, T. V. Pogorelov, E. Tajkhorshid, S. Park, J. B. Klauda and W. Im, CHARMM-GUI HMMM Builder for Membrane Simulations with the Highly Mobile Membrane-Mimetic Model, *Biophys. J.*, 2015, **109**(10), 2012–2022.
29 E. L. Wu, X. Cheng, S. Jo, H. Rui, K. C. Song, E. M. Davila-Contreras, Y. Qi, J. Lee, V. Monje-Galvan, R. M. Venable, J. B. Klauda and W. Im, CHARMM-GUI Membrane Builder toward realistic biological membrane simulations, *J. Comput. Chem.*, 2014, **35**(27), 1997–2004.
30 A. Chugunov, D. Pyrkova, D. Nolde, A. Polyansky, V. Pentkovsky and R. Efremov, Lipid-II forms potential "landing terrain" for lantibiotics in simulated bacterial membrane, *Sci. Rep.*, 2013, **3**, 1678.
31 E. R. Turpin, S. Mulholland, A. M. Teale, B. B. Bonev and J. D. Hirst, New CHARMM force field parameters for dehydrated amino acid residues, the key to lantibiotic molecular dynamics simulations, *RSC Adv.*, 2014, **4**(89), 48621–48631.
32 J. Huang, S. Rauscher, G. Nawrocki, T. Ran, M. Feig, B. L. de Groot, H. Grubmuller and A. D. MacKerell Jr., CHARMM36m: an improved force field for folded and intrinsically disordered proteins, *Nat. Methods*, 2017, **14**(1), 71–73.
33 W. Jiang, J. C. Phillips, L. Huang, M. Fajer, Y. Meng, J. C. Gumbart, Y. Luo, K. Schulten and B. Roux, Generalized Scalable Multiple Copy Algorithms for Molecular Dynamics Simulations in NAMD, *Comput. Phys. Commun.*, 2014, **185**(3), 908–916.
34 W. Humphrey, A. Dalke and K. Schulten, VMD: visual molecular dynamics, *J. Mol. Graphics*, 1996, **14**(1), 33–38.
35 R. Pokhrel, E. Pavadai, B. S. Gerstman and P. P. Chapagain, Membrane pore formation and ion selectivity of the Ebola virus delta peptide, *Phys. Chem. Chem. Phys.*, 2019, **21**(10), 5578–5585.
36 J. He, L. I. Melnik, A. Komin, G. Wiedman, T. Fuselier, C. F. Morris, C. G. Starr, P. C. Searson, W. R. Gallaher, K. Hristova, R. F. Garry and W. C. Wimley, Ebola Virus Delta Peptide is a Viroporin, *J. Virol.*, 2017, **91**(16), e00438-17.
37 B. C. Zhao, H. C. Lin, D. Yang, X. Ye and Z. G. Li, Disulfide Bridges in Defensins, *Curr. Top. Med. Chem.*, 2015, **16**(2), 206–219.
38 A. A. Bahar and D. Ren, Antimicrobial peptides, *Pharmaceuticals*, 2013, **6**(12), 1543–1575.
39 J. Kofinger, G. Hummer and C. Dellago, Single-file water in nanopores, *Phys. Chem. Chem. Phys.*, 2011, **13**(34), 15403–15417.
40 G. Hummer, J. C. Rasaiah and J. P. Noworyta, Water conduction through the hydrophobic channel of a carbon nanotube, *Nature*, 2001, **414**(6860), 188–190.

41 R. Pomes and B. Roux, Molecular mechanism of H^+ conduction in the single-file water chain of the gramicidin channel, *Biophys. J.*, 2002, **82**(5), 2304–2316.
42 J. A. Dani and D. G. Levitt, Water transport and ion-water interaction in the gramicidin channel, *Biophys. J.*, 1981, **35**(2), 501–508.
43 T. W. Allen, O. S. Andersen and B. Roux, Energetics of ion conduction through the gramicidin channel, *Proc. Natl. Acad. Sci. U. S. A.*, 2004, **101**(1), 117–122.
44 T. Bastug and S. Kuyucak, Energetics of ion permeation, rejection, binding, and block in gramicidin A from free energy simulations, *Biophys. J.*, 2006, **90**(11), 3941–3950.
45 P. Agre, Aquaporin Water Channels (Nobel Lecture), *Angew. Chem., Int. Ed.*, 2004, **43**(33), 4278–4290.
46 J. A. Kers, R. E. Sharp, S. Muley, M. Mayo, J. Colbeck, Y. Zhu, A. W. DeFusco, J. H. Park and M. Handfield, Blueprints for the rational design of therapeutic mutacin 1140 variants, *Chem. Biol. Drug Des.*, 2018, **92**(6), 1940–1953.
47 A. Horner, F. Zocher, J. Preiner, N. Ollinger, C. Siligan, S. A. Akimov and P. Pohl, The mobility of single-file water molecules is governed by the number of H-bonds they may form with channel-lining residues, *Sci. Adv.*, 2015, **1**(2), e1400083.
48 V. J. van Hijkoop, A. J. Dammers, K. Malek and M. O. Coppens, Water diffusion through a membrane protein channel: a first passage time approach, *J. Chem. Phys.*, 2007, **127**(8), 085101.
49 S. W. Chiu, S. Subramaniam and E. Jakobsson, Simulation study of a gramicidin/lipid bilayer system in excess water and lipid. II. Rates and mechanisms of water transport, *Biophys. J.*, 1999, **76**(4), 1939–1950.
50 M. T. Lee, W. C. Hung, F. Y. Chen and H. W. Huang, Mechanism and kinetics of pore formation in membranes by water-soluble amphipathic peptides, *Proc. Natl. Acad. Sci. U. S. A.*, 2008, **105**(13), 5087–5092.
51 J. Medeiros-Silva, S. Jekhmane, E. Breukink and M. Weingarth, Towards the native binding modes of lipid II targeting antibiotics, *ChemBioChem*, 2019, DOI: 10.1002/cbic.201800796.
52 T. Giorgino, Computing 1-D atomic densities in macromolecular simulations: the density profile tool for VMD, *Comput. Phys. Commun.*, 2014, **185**(1), 317–322.
53 R. R. Bonelli, T. Schneider, H. G. Sahl and I. Wiedemann, Insights into *in vivo* activities of lantibiotics from gallidermin and epidermin mode-of-action studies, *Antimicrob. Agents Chemother.*, 2006, **50**(4), 1449–1457.
54 B. de Kruijff, V. van Dam and E. Breukink, Lipid II: a central component in bacterial cell wall synthesis and a target for antibiotics, *Prostaglandins, Leukotrienes Essent. Fatty Acids*, 2008, **79**(3-5), 117–121.
55 E. Breukink, I. Wiedemann, C. van Kraaij, O. P. Kuipers, H. G. Sahl and B. de Kruijff, Use of the cell wall precursor lipid II by a pore-forming peptide antibiotic, *Science*, 1999, **286**(5448), 2361–2364.